Selection of polymer segment species matters for electrolyte properties and performance in lithium metal batteries

*Min-Huei Chiou[a], Elisabeth Verweyen[a], Diddo Diddens[a], Lennart Wichmann[a], Christina Schmidt[a], Kerstin Neuhaus[a], Aditya Choudhary[b], Dmitry Bedrov[b], Martin Winter[a,c], Gunther Brunklaus[a]**

[a] Forschungszentrum Jülich GmbH, Helmholtz-Institute Münster, IEK-12, Corrensstraße 46, 48149 Münster, Germany

[b] Department of Materials Science and Engineering, University of Utah, 122 S. Central Campus Dr., Salt Lake City, UT 84112, USA

[c] MEET Battery Research Center, University of Münster, Corrensstraße 46, 48149 Münster, Germany

* Email: g.brunklaus@fz-juelich.de

Keywords: membrane homogeneity, phase separation, consistency of ion transport, lithium deposition, polarity compatibility, copolymer, plasticizer distribution

Abstract

Control of homogeneous lithium deposition governs prospects of advanced cell development and practical applications of high-energy-density lithium metal batteries. Polymer electrolytes are thus explored and employed to mitigate the growth of high surface area lithium species while enhancing the reversibility of the lithium reservoir upon cell cycling. Herein, an in-depth understanding of the distribution of membrane properties and lithium deposition behavior affected by the selection of polymer segment species is derived. It is demonstrated that severely localized lithium deposits featuring needle-like morphologies may be readily observed when electrostatic fields (or partial charges) and the amount of Li^+ coordinators of the primary and secondary polymer segment species appear rather dissimilar, leading to a sudden cell failure at early stages of cell operation. In comparison, employment of optimized copolymer electrolytes enables superior cell performance at 1 C even with thicker cathodes (6.3 mg cm^{-2}). Additionally, the improvement of cell cycling stability due to enhancement of similarity of dipole moments and partial charge distributions among copolymer segments are also demonstrated for different polymer systems, contributing to avoidance of undesired lithium protrusions; also reflecting a viable concept for the design of future copolymer electrolytes.

Introduction

On a mission to transform energy storage, next-generation solid-state lithium metal batteries (LMBs) affording high safety and enhanced energy density are expected to govern the vehicle market after the year 2030 (Battery2030+). In addition to integration of complex technology, a major challenge of such batteries constitutes reliable control and achievement of homogeneous lithium deposition. In this respect, polymers possessing prominent features, including e.g. sufficient compressive mechanical properties, good affinity and contacts against the electrodes and durable electrochemical stability towards lithium metal, are considered as highly suitable electrolyte candidates that eventually mitigate the growth of high surface area lithium (HSAL) deposits.[1] However, some other factors which potentially trigger inhomogeneous distribution of current density, ultimately leading to dendrite growth upon cycling, should be also taken into account, including but not limited to the lithium host materials, anode interphases and bulk electrolytes. Several approaches for amelioration of cell performance have been demonstrated from the perspective of host materials and interphase properties, such as employments of 3D skeleton structures as lithium host,[2] in this way regulating the distribution of current density near the lithium surfaces, and exploitation of artificial solid electrolyte interphase (SEI) to stabilize and homogenize the interface between the electrode and electrolyte.[3, 4] Also, the impact of electrolyte concentration gradients and mechanical features towards resulting morphologies of lithium deposits were critically discussed based on models of Chazalviel or Monroe and Newman, respectively, emphasizing that polymer electrolytes with high Li^+ transference number (e.g. system of single-ion conducting polymers) and mechanical modulus (e.g. range of MPa) can effectively suppress formation of HSAL deposits.[5, 6] However, the presence of (localized) electrolyte membrane inhomogeneity that eventually could adversely affect the behavior of lithium deposits

upon cycling is often ignored and not systematically explored, especially not in case of copolymer systems.

To boost salient features of common homopolymer electrolytes, additives, plasticizers or other polymer species are often introduced, affording synergistic effects, such as suitable balance of mechanical stability and ionic conductivity. [7, 8] Note that different polymer architectures provide individual ion speciation based on lithium-ion coordination with functional groups and mobile components, thereby govering the overall ion transport capability within the materials (e.g. due to ion hopping, polymer segmental motion, or exchange among coordination shell constituents)[9]. Nevertheless, general guidance for designing mixed electrolytes is still incomprehensive and in practice might lead to defects of electrolyte microstructures. For instance, in case of block copolymer systems, at least two incompatible or partially compatible polymer segments composed of independent monomers are exploited to attain micro-phase separation, thereby offering defined functional domains; some of them enable the formation of continuous pathways dominating charge carrier transport (called salt solvating polymer block established by polar groups such as –O–, C=O, –N–, –S–, or C=N),[9] and the others solely enhance the mechanical rigidity (mechanically robust but ion insulating block).[10] Pronounced phase separation or uncontrollable agglomeration and orientation of these domains may trigger uneven electrodeposition of lithium metal and occurrence of local defects especially upon the exposure to a critical current density, which however tends to be neglected even though the differences of local ionic conductivity are obviously recognizable.[11-13] In a current study, it was elucidated that the behavior of heterogeneous lithium deposits is strongly associated with membrane phase separation in case of polymer blend systems, and though the invoked concept appears applicable to other block copolymers or ceramic hybrid electrolytes, no insightful details of structural chemistry were discussed.[14]

Apart from polymer blends or block copolymers, a local disparity of charge carrier transport could also emerge in the system of "random" (cross-linked) copolymers (e.g. asymmetric copolymer)[15] when the chemical structures and entities of the introduced monomers/oligomers have disparate lithium-ion coordination sites or appear incompatible in view of polarity, thereby eventually giving rise to molecular aggregation and rather non-uniform distribution of electrolyte properties.[16] This inconsistency of ion transport could detrimentally cause cell cycling instabilities. Moreover, in plasticized (gel) polymer systems, plasticizer is mainly used to boost overall conductivity, but the polarity divergences within the polymer membranes might additionally govern the resulting inhomogeneity of any plasticizer distribution that potentially triggers even more hazards based on the formation of severely agglomerated lithium deposits upon electrochemical cycling.[13] As indicated from **Figure 1**, LMB cell performances with the published gel polymer electrolytes that contain "incompatible" polymer segments are overall limited by slow cycling rates and short cycle numbers. Notably, recently reported electrolyte materials that afford promising cycling behaviors mostly have "compatible" copolymer network structures. But so far, no research has put attention on this interrelation.

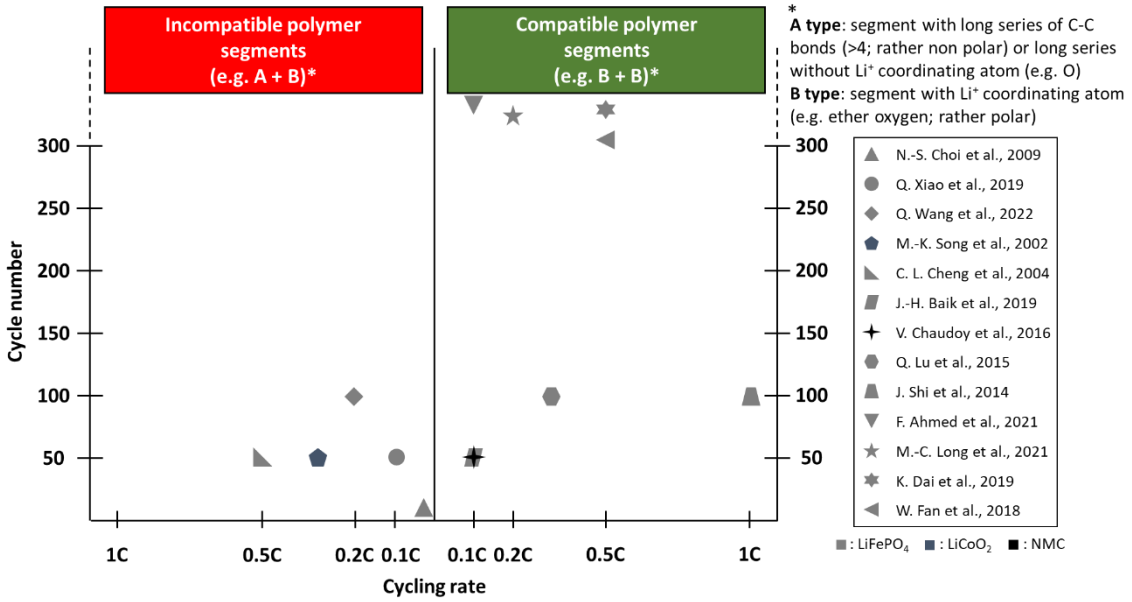

Figure 1. LMB cell performance (longevity) of gel polymer electrolytes containing at least two different polymer segments.[17-29]

In the present work, the impact of compatibility based on copolymer structural chemistries (e.g. electrostatic potentials) on membrane homogeneity and electrochemical cycling performance of cells are investigated. A multi-functional and carbonate-based oligomer (modified poly(trimethylene carbonate)-grafted cyclodextrins (PTMC-GCDs)) was introduced as primary segment species due to its amorhpous structure and promising electrochemical features (including high transference number of ~0.6 and wide oxidative stability window of up to 5 V, as revealed by previous work),[30] and several types of monomer species with distinct chemical bonds and polarities were explored as secondary segment species to establish various network structures in the presence of plasticizer or mobilizer, while systematically evaluating the corresponding electrolyte properties and electrochemical features in NMC622||Li and Cu||Li type cells. Notably, behaviors of molecular aggregations and lithium-ion coordination can be clearly elucidated by AFM images and molecular dynamics (MD) simulations. In combination with SEM images and solid-state NMR data, the results indicate that the deposited lithium morphology is strongly associated with the polymer membrane homogeneity, as mainly determined by the actual structural

compatibility between both the primary and secondary segment species. Namely, very dissimilar molecular electrostatic fields (or partial charges) among the considered electrolyte constituent species likely result in severely localized lithium deposition and unanticipated cell failures upon electrochemical operation. Same behaviors can be also observed in the PEO-based system. Thus, parameters for the rational design of electrolytes in plasticized (cross-linked) copolymer systems are reconsidered, including the enhancement of membrane homogeneity and the consistency of achievable charge carrier transport which can be further elevated by increasing the similarity of molecular electrostatic fields among the utilized polymer species.

Experimental Section

Material

The multi-functional carbonate-based oligomers (modified PTMC-grafted α-Cyclodextrins; Mn ~11k) with 90% modification at the terminal groups (hydroxyl group to acrylate) were prepared according to a reported procedure (please see ^{1}H NMR and GPC data collected in Figure S1, Supporting Information).[30] 1,6-Hexanediol diacrylate (HDDA, 99%, dried over 4 Å molecular sieves) and Triethylene glycol diacrylate (TEGDA, 90%, dried over 4 Å molecular sieves) were received from abcr GmbH. 2,2-Dimethoxy-2-phenylacetophenone (DMPA, 99%), Poly-(ethylenglykol)-diacrylat (PEGDA; Mn 700), 2-(2-Ethoxyethoxy) ethyl acrylate (EOEOEA, dried over 4 Å molecular sieves) and 1,3-Butanediol diacrylate (BDDA, >98%, dried over 4 Å molecular sieves) were purchased from Sigma Aldrich, Germany. Propylene carbonate (PC) and lithium bis-trifluoro-methane-sulfonimide (LiTFSI) were obtained from BASF and Solvionic, respectively. $LiNi_{0.6}Mn_{0.2}Co_{0.2}O_2$ (NMC622) cathode sheets (with a mass loading of 2.5 mg cm^{-2} and layer thickness of 17 μm) were prepared following established protocols,[30] and a thicker NMC622 cathode sheet (6.3 mg cm^{-2}) was purchased from CUSTOMCELLS.

Preparation of quasi-solid copolymer electrolyte

According to previous work,[30] a high fraction of secondary species would lead to lower capacity retention of cells operated with these carbonate-based polymer electrolytes. Thus, the mass ratio between primary (modified PTMC-GCDs) and secondary species was set to 3:1. PC was selected as an optimized plasticizer in this PTMC-based electrolyte system due to its superior cycling performance compared to other carbonate-based solvents, such as DMC and EC/PC with or without FEC additives, which has been also demonstrated in our old work. A viscous fluid comprised of 25.7 wt% carbonate-based multi-functional oligomer (primary segment species), 8.6 wt% monomer (secondary segment species), as well as 24.2 wt% LiTFSI, 40.9 wt% PC and 0.6 wt% DMPA was casted between two mylar foils with a gap of 130 µm after blending. The mixture was photo-cured for 90 min in an UVACUBE 100 to ensure complete cross-linking (absence of C=C bonds).[30] In total, five quasi-solid and cross-linked electrolyte samples were explored, containing PTMC homopolymer (1), TEGDA (2), EOEOEA (3), HDDA (4) and BDDA (5) copolymers. (see in **Scheme 1** and network formation in Scheme S1, Supporting Information).

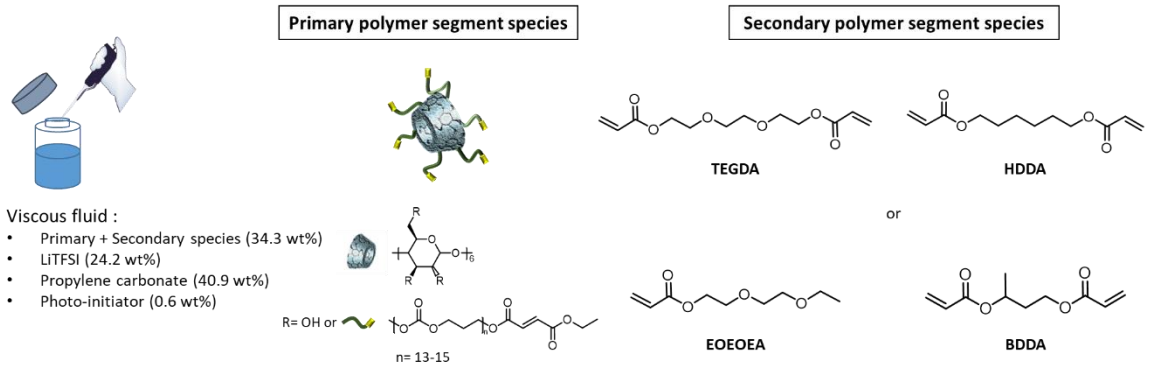

Scheme 1. Electrolyte constituents and structures of multi-functional oligomers (primary species) and different configurations of the considered monomers (secondary species).

PEO-based plasticized electrolytes were prepared in the same way, but replacing modified PTMC-GCDs by PEGDA (Mn 700) as the primary segment species.

Material characterization

Electrostatic potential

To quantify the polarity of the individual polymer and plasticizer species, density functional theory (DFT) calculations were carried out with the program Gaussian 16.[31] All calculations were performed at B3LYP/def2-TZVP level of theory including the implicit SMD solvation model with built-in parameters for acetone,[32] which has a similar dielectric constant as typical liquid carbonate electrolytes.[33-35] For all optimized geometries, the electron density and electrostatic potentials were computed. More details including the computation of partial charge are given in Figure S2 and Table S1 (Supporting Information).

Rheology

A modular compact rheometer (MCR102) from Anton Paar equipped with a measuring system of PP15-SN71066 (diameter of 15 mm) was utilized to determine the mechanical properties of the polymer membranes. The amplitude (γ) was fixed to a constant value of 0.5%, and the angular frequency was varied in the range of 200 to 1 rad s^{-1} while 1N of normal force was applied.

Scanning electron microscopy

SEM analysis was invoked to assist the inspection of lithium surface morphologies and lithium deposits in the presence of polymer membranes and Cu substrate. Multiple areas of each sample were analyzed at an Auriga CrossBeam workstation from Carl Zeiss (Germany), exploiting an acceleration voltage of 3 kV.

Atomic force microscopy (AFM)

All AFM measurements were performed using a Cypher-ES AFM (Asylum Research by Oxford Instruments, UK) with PPP-NCSTPt probes (Nanosensors, Switzerland). The probes show a nominal force constant in the range of 7.4 N m^{-1} and are coated with a Pt/Ir alloy to ensure conductivity for Kelvin Probe Force Microscopy (KPFM) measurements. All the samples were

stored and examined in air. For topography measurements, the phase shift of the mechanical excitation of the cantilever and local surface potential were done simultaneously in a two-pass experiment in intermittent contact. The mode that enables surface potential measurements is referred to as Kelvin Probe Force Microscopy.[36] For this, the AFM tip is scanned above the surface in a defined height of 30 nm, and the contact potential difference between the metal coated tip and sample is recorded, which is equivalent to a local surface potential of the considered samples. For image analysis, the program MountainsSPIP Starter 8.0 (Digital Surf, France) was employed.

Molecular dynamics (MD) simulations

Atomistic MD simulations were conducted using Atomistic Polarizable Potential for Liquids, Electrolytes & Polymers (APPLE&P) using in-house developed simulation package.[37, 38] This polarizable force field has been extensively used to investigate polymer electrolytes.[39-41] In this force field, each force center has an isotropic polarizability, and the induced point dipoles are computed using the self-consistent approach. We used the Thole screening factor of 0.2 to prevent "polarization catastrophe".[42] All the bonds were constrained using the SHAKE algorithm.[43] The cut-off distance of 15.0 Å was used to calculate the van der Waals and the real part of electrostatic interactions. The Ewald summation method was utilized to compute the reciprocal part of electrostatic interaction. During the simulation, temperature and pressure were controlled using Nose−Hoover thermostat with a frequency of 0.01 fs^{-1} and Anderson−Hoover barostat with a frequency of 0.0005 fs^{-1}.[44, 45] A multiple-time integration scheme was incorporated to enhance the computational efficiency.[46] The small timestep of 0.5 fs was used for calculating bonds and bends; the medium timestep of 1.5 fs for calculating torsions and the short-range (< 8.0Å) non-bonded interactions; and the large timestep of 3.0 fs was used for calculating the long-range non-bonded interactions (> 8.0Å) and the reciprocal part of the Ewald summation.

Two sets of systems were investigated. In the first set, the additives (namely secondary segment species) were not part of the polymer and were dissolved in the solvent; while in the second set, the additive end were assumed to react with polymer forming a comb-branched chain with side chains being a mixture of PTMC and corresponding additive. The objectives of simulating two sets are to understand the behavior of additives before the polymerization begins and after the completion of polymerization. In both cases, the molar ratio of PTMC:TEGDA:Li^+:TFSI:PC is 6:14:34:34:162 and PTMC:HDDA:Li^+:TFSI:PC is 6:15:34:34:162. In initial configurations, all molecules were randomly placed in a large cubic simulation box of size 300 Å. The dimension of the box was shrunk over 3 ps to achieve a density of about 1 g/cc. The obtained system was run in NVT ensemble at a high temperature (500K) for 3 ns to allow relaxation of polymer degrees of freedom. Then the systems were cool down to 300 K, followed by an equilibration run in the NPT ensemble for 3 ns. Production runs were over 10 ns in the NPT ensemble. Additional details including comparability of linear and grafted CD systems are given in the Table S2 and Figure S3 (Supporting Information).

^{7}Li solid-state nuclear magnetic resonance

Coin cells (diameter of 10 mm) of Cu||Li (1M HCl treated Cu) as well as NMC622||Li were analyzed with respect to deposited lithium morphologies after electrochemical cell operation. Static ^{7}Li NMR experiments were performed at room temperature employing an AVANCE III 200 MHz spectrometer operating at a magnetic field of 4.7 T with a ^{7}Li Larmor frequency of 77.9 MHz. All the NMR spectra were recorded with a saturation recovery sequence at a pulse length of 15 µs, a relaxation delay of 0.5 s, averaging 2048 scans for each spectrum. The ^{7}Li NMR spectra were referenced with respect to 1M LiCl solution (^{7}Li, 0 ppm). Data analysis was done with BRUKER Topspin 3.5 software applying automatic phase correction. The total signal intensity of the peaks

reflecting Li metal species was integrated over the chemical shift range from 180 to 330 ppm, and fitted considering three distinct lithium metal species.[47]

Electrochemical characterization

Lithium-ion conductivity

The fractional conductivity of lithium ions was derived from the overall ionic conductivity multiplied with Li^+ transference number. Electrochemical impedance spectroscopy (EIS) was conducted to derive overall ionic conductivities using an Autolab device. Polymer membranes were punched to a 12 mm diameter disks (thickness of 100-150 µm) and assembled in coin cells (CR2032) between two polished stainless-steel electrodes. Here, temperature ranges of 0 °C to 70 °C with 10 °C increment per step scanning over a frequency range from 1 Hz to 1 MHz with a 10 mV sinus amplitude after a preheating step (20 °C to 70 °C) was applied. The transference numbers were examined in Li||Li cells at 20, 40 and 60 °C, respectively, after a duration of one-day equilibration of all the samples at the moderate temperature of 40 °C. A DC polarization voltage (ΔV) of 10 mV was applied for potentiostatic polarization, the resulting current was recorded over time, and corresponding impedance spectra were collected between 1 Hz and 1 MHz before and after polarization. For data analysis, assuming negligible ion-ion interactions, an approach proposed by Watanabe et al. was exploited since the interfacial resistance does not notably vary after cell polarization.[48]

Cell assembly and cycling conditions

NMC622||Li cells were built in a two-electrode coin-cell configuration in a dry room (dew point below -66 °C). The diameters of the anode, cathode and polymer electrolytes were set to 14 mm, 10 mm and 12 mm while the layer thicknesses were 300 µm, 37 µm (including 20 µm of Al foil; mass loading of 2.5 mg cm^{-2}) and 100-130 µm, respectively. A Mylar-foil ring (outer diameter:

16 mm; inner diameter: 13 mm) was placed at the outer area of the polymer electrolyte to cover residual lithium metal to avoid short circuit. In addition, Cu||Li (1M HCl treated Cu) were also assembled, following the same sandwich method as above described. All the cells were cycled on Maccor 4000 battery analysis system (USA) at 20 °C and 60 °C, respectively, and NMC622||Li were operated at a voltage range of 4.3 V and 3 V (constant current, theoretical specific capacity of 180 mAh g^{-1}).

Results and discussion

Impact of selection of secondary polymer species on membrane homogeneity

To consider the influence of structural and polar differences between primary and secondary polymer species as well as the resulting inhomogeneous electrolyte properties within formed membranes and limited electrochemical cell performance of "quasi-solid" copolymer electrolytes, we investigated PTMC-based polymer electrolytes. Herein, multi-functional PTMC-GCDs comprise the primary polymer species while several monomers with different chemical bonds are individually introduced as secondary polymer species, involving TEGDA, EOEOEA and HDDA (as shown in **Figure 2**). Notably, the electrolytes (2)-(4) are composed of primary and different secondary species that establish distinct copolymer networks in the presence of LiTFSI and plasticizer (propylene carbonate (PC)), while electrolyte (1) is plasticized and cross-linked PTMC homopolymer. DFT calculations reveal that a series of C-C bonds (6 neighboring carbons in row) in HDDA appears rather non-polar compared to segments of TEGDA and EOEOEA containing few ether oxygens (C-C-O), thereby offering different degrees of compatibility with PTMC-GCDs, as determined by the similarity of electrostatic fields (or partial charges) among polymer segments.[19] Overall, electrolyte components of PTMC-GCDs, PC and secondary species involving C-C-O bonds (e.g. TEGDA and EOEOEA) occur as relatively polar species which have

larger differences of electron densities/partial charges among neighboring atoms (see Figure 2, data of patrial charge shown in Figure S2 and Table S1, Supporting Information). Hence, the selection among these various mono/bifunctional monomers used as secondary polymer species could in principle impact compatibility between copolymer segments and lead to structural heterogeneities in membrane and affect LMB cell performance.

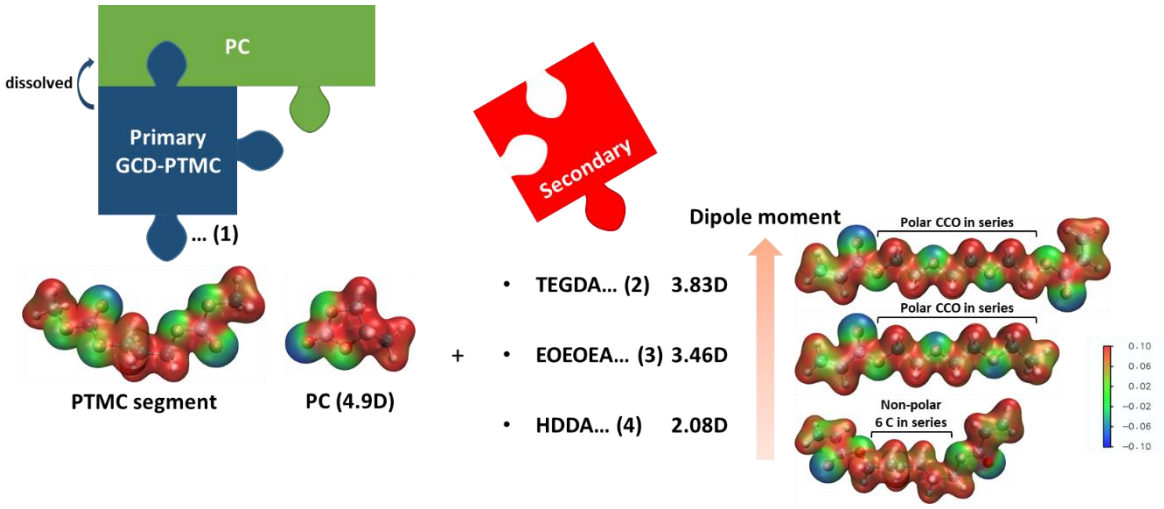

Figure 2. Components of the introduced electrolytes (1)-(4), containing plasticized and cross-linked homopolymer (1), TEGDA copolymer (2), EOEOEA copolymer (3) and HDDA copolymer (4), respectively. Calculated electrostatic potentials around atoms of PTMC segment, propylene carbonate and the considered secondary oligomer species (in their extended conformation) as obtained from DFT calculations.

To monitor membrane homogeneity, AFM constitutes a powerful tool that provides information of polymer membrane topography, including surface roughness and potential, elasticity/adhesion, and so on.[49, 50] In **Figure 3**a-d, the comparison between phase images of each electrolyte clearly illustrates that the membrane of electrolyte (4) has rather strong color contrasts established by mechanically harder areas (small phase shift, darker) and comparatively softer domains (high phase shift, lighter), thus unambiguously highlighting inconsistent mechanical elasticity or adhesion present within the polymer membrane. This kind of extreme phase change is, however, absent in the other electrolyte materials. Besides, though topography images reveal all membrane surfaces are generally flat (see **Figure 3**e, cases of electrolyte (2) and (3) shown in Figure S4a-b, Supporting Information), sharply defined elevated spots (light brown) can be readily

observed in case of electrolyte (4), exhibiting differences at the z-axial scale on the order of 20 nm. The 3D overlapped AFM image also discloses a good match between those domains in topography and phase shift, showing that the soft domains are only located at the surface depressions (see **Figure 3**f). This domain pattern presumably results from two incompatible segments of PTMC and HDDA that foster molecular agglomeration during blending or cross-linking/polymerizing the electrolyte precursors (solubility of PTMC-GCDs in various secondary segment species is shown in Figure S5, Supporting Information), even though the final DSC analysis in Figure S6 (Supporting Information) reflects only one glass transition temperature.[51, 52] In addition, the image of surface potential displays that the charges seem to be well distributed (**Figure 3Fehler! Verweisquelle konnte nicht gefunden werden.**g), yet the areas possessing higher surface potential (red color) mostly show up at the surface depressions (soft domain), whereas lower potential areas represent harder domains, also reflecting changes of local electrolyte composition.

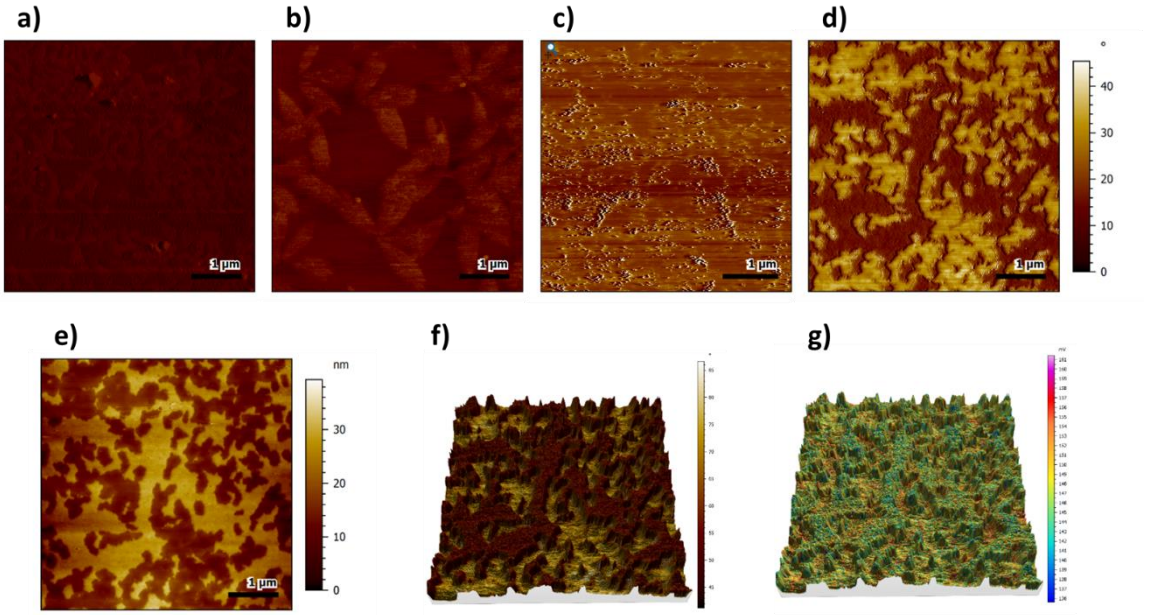

Figure 3. a-d) AFM phase images of electrolytes (1)-(4), respectively; small artifacts (stripes) exist in c) caused by stuck cantilever at the polymer membrane due to the surface stickiness. e) Topography image of electrolyte (4). f) Three-dimensional overlapped image of topography and phase shift and g) 3D overlapped image of topography and surface potential.

To better understand the underlying molecular scale interactions and correlations that can lead to observed heterogeneity in membrane, atomistic MD simulations were conducted for several

related systems. The first set of systems was comprised of linear PTMC, representing primary polymer species, and the corresponding additives used as the secondary segment species (HDDA or TEGDA), PC solvent and Li-salt with compositions corresponding to experimental ratios. We refer to these systems as L-PTMC/Additive/PC. These systems are representing the molecular interactions in the initial stages of membrane formation before polymerization reactions progress, and the systems can be considered as solutions. **Figure 4**a, shows a snapshot of one of such system highlighting the distribution of an additive (TEGDA) and the Li^+ ions. As shown in Figure 2, each component in the system contains O atoms with negative partial charges. Double bonded O atoms in PC, PTMC, TFSI, and end-groups of additives as well as the ether oxygens (e.g. in TEGDA) are the primary source of atoms with negative partial charges that will preferentially interact with Li^+ and form its' coordination shell. Analysis of radial distribution functions allows to characterize the composition of Li^+ first coordination shell (defined as 3.0 Å from the Li^+ center). On average, each Li^+ contains about 4.3-4.5 O atoms in the first coordination shell. However, as illustrated in **Figure 4**b and c, all species are contributing to Li^+ coordination as initial solution is mixed. The table in Figure 4b, illustrates the average number of each oxygen type contributing to Li^+ coordination, while panels in Figure 4c provide probability distributions of finding a specific number of oxygens of a given type in the coordination shell. The double-bonded O atoms from PC solvent contribute almost half of the coordination shell, while PTMC, TFSI, HDDA or TEGDA have comparable contributions. In the system without any additives, PTMC has about 1.3 O atoms in the Li^+ coordination while TFSI contributes only 0.7 oxygens which is consistent with the high degree of dissociation of LiTFSI salt in these electrolytes. As HDDA or TEGDA are added to the system, their end group double-bonded oxygens can compete for coordination with Li^+ and replace some fraction of PC and PTMC oxygens. For example, in the L-PTMC/HDDA/PC system, the coordination by PTMC and PC reduces from 1.3 to 0.75 and from 2.3 to 2.0, respectively, allowing

about 0.8 O of HDDA in the Li^+ coordination. The relatively high negative charge of the double-bonded O entities and their steric exposure in the end-groups of HDDA and TEGDA makes these entities efficient contributors to cation coordination.

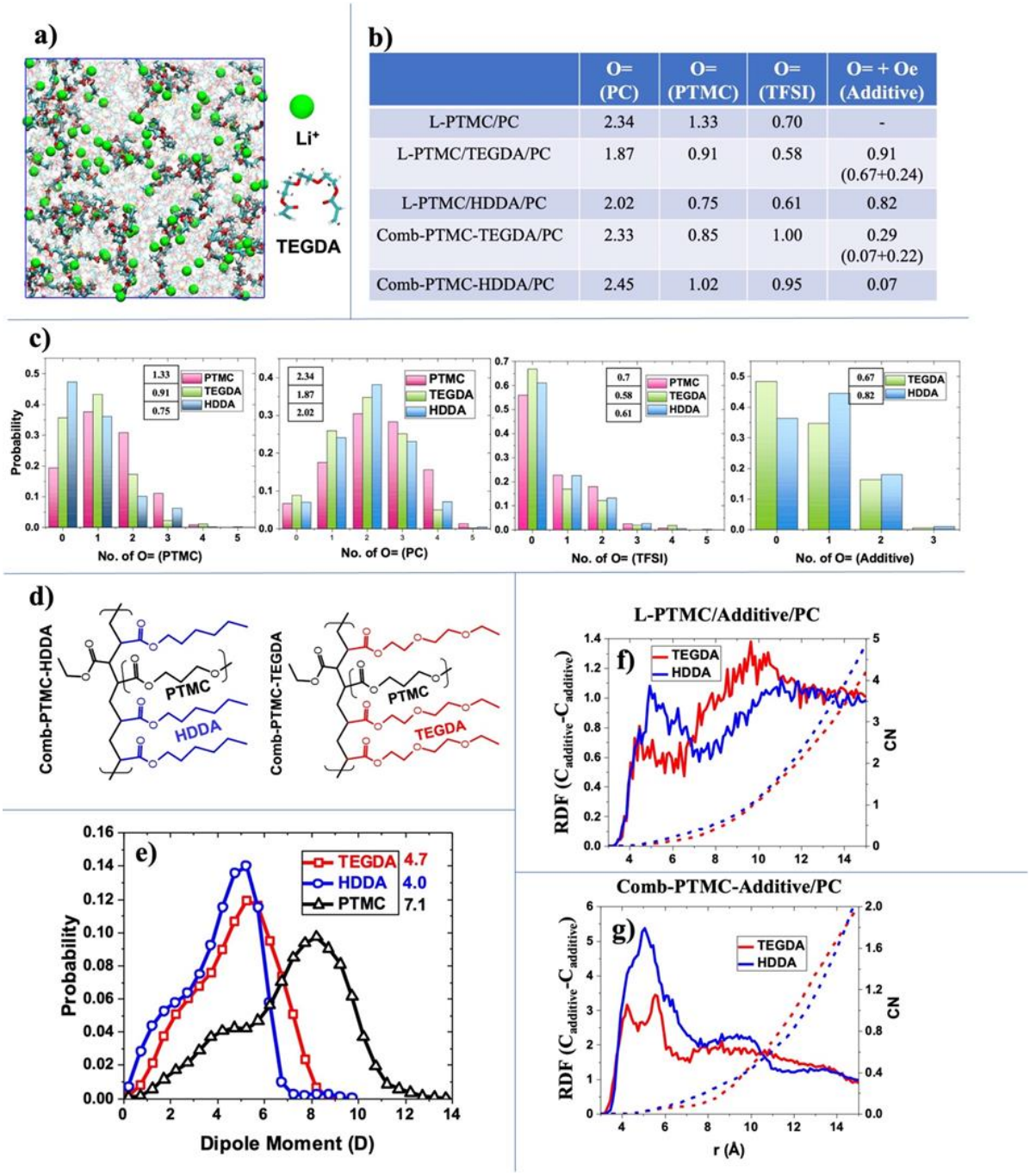

	O= (PC)	O= (PTMC)	O= (TFSI)	O= + Oe (Additive)
L-PTMC/PC	2.34	1.33	0.70	-
L-PTMC/TEGDA/PC	1.87	0.91	0.58	0.91 (0.67+0.24)
L-PTMC/HDDA/PC	2.02	0.75	0.61	0.82
Comb-PTMC-TEGDA/PC	2.33	0.85	1.00	0.29 (0.07+0.22)
Comb-PTMC-HDDA/PC	2.45	1.02	0.95	0.07

Figure 4. Results from MD simulations: a) Snapshot of L-PTMC/TEGDA/PC/LiTFSI system with Li^+ and TEGDA molecules highlighted; b) Average number of O atoms in the Li^+ first coordination shell; c) Probability distribution of funding a certain number of O atoms of different types in Li^+ coordination in L-PTMC/Additive/PC electrolytes (Notation: "PTMC" = L-PTMC/PC electrolyte, "TEGDA" = L-PTMC/TEGDA/PC, "HDDA" = L-PTMC/HDDA/PC); d) schematic illustration of comb-branched polymers representing polymerized membrane; e) Distribution of instantaneous molecular dipole moments of components obtained

from MD simulation trajectories (PTMC considers a dipole moment of two consecutive monomers in the chain); f) and g) Carbon-carbon radial distribution function of HDDA or TEGDA in L-PTMC/Additive/PC and Comb-PTMC-Additive/PC systems.

As polymerization reaction takes place and the double bonds of additives and PTMC end groups react, the local environment near the double-bonded O atoms changes and becomes more sterically crowded. To mimic this effect, we have simulated systems containing comb-branched chains as illustrated in **Figure 4**d, in which the end groups of additives and PTMC were assumed to underwent the polymerization reaction involving C=C bonds (systems referred as Comb-PTMC-Additive/PC). As a result, the negatively charged oxygen atoms in the oligomer end groups are now having notably more steric interference from the backbone and neighboring groups. Simulations of Comb-PTMC-HDDA/PC and Comb-PTMC-TEGDA/PC systems with the same salt concentration reveal that once HDDA or TEGDA additives become part of the network, their ability to coordinate Li^+ drops substantially. Figure 4b shows that the average number of double-bonded O atoms of HDDA and TEGDA coordinating Li^+ drops by an order of magnitude (compared to free additives systems) and becomes less than 0.1. The coordination of Li^+ with ether O of TEGDA remains similar as in the system with free additives, hence still allowing TEGDA segments to participate in cation coordination.

The observed change in Li^+ coordination between initial solution and expected resulting polymeric structures comprising membrane further emphasizes the complexity of membrane design and fabrication. Favorable interaction of Li-salt with some components and less favorable with others can create additional thermodynamic forces to drive structural heterogeneities. To further assess the compatibility of considered components, we have calculated a distribution of the dipole moments of HDDA and TEGDA additives, as well as PTMC segment of similar length (two repeat units). The dipole moments shown in Figure 2 were calculated for a single, extended state conformation. However, these molecules/segments are conformationally flexible, and therefore we used configurations from MD simulations to calculate the distributions of instantaneous dipole

moments and the corresponding averages. **Figure 4**e illustrates that all key components show a broad range of dipole moments, with TEGDA averaging 4.7D, which is very close to PC dipole moment of 4.9D,[19] while HDDA molecule has about 20% lower dipole moment (around 4.0D). The effectively lower dipole moment of HDDA combined with the discussed above inability to contribute to the Li^+ coordination after polymerization, will likely make the HDDA segments thermodynamically less compatible with other components (PTMC and PC) and hence creating driving forces for HDDA segregation. TEGDA segments, while also lose the ability to contribute the double-bonded O atoms to Li^+ coordination after polymerization, their intrinsic higher dipole moment and the presence of ether O atoms still contributing to cation coordination make them more compatible in these electrolytes. To support this argument, we have analyzed the $C_{additive} - C_{additive}$ radial distribution function (RDF) in the L-PTMC/Additive/PC and Comb-PTMC-Additive/PC systems (**Figure 4**f and g). In electrolytes with free additives (i.e. before polymerization), the HDDA and TEGDA molecules have similar distributions not showing any noticeable aggregation (RDF is around 1.0 indicating a homogeneous spatial distribution). However, in the Comb-PTMC-Additive/PC systems, a noticeably larger aggregation of HDDA segments is observed compared to TEGDA segments. These trends are consistent with AFM observed heterogeneities discussed above.

Cycling performance, electrochemical and physical features of electrolytes

In the light of achieving high-energy-density LMB cells, NMC622 cathode that offers higher capacity is employed for the evaluation of cell performance in this work.[53] In **Figure 5**a, the cycling result displays that electrolytes (1) and (4) in principal deliver higher discharge capacities (100 mAh g^{-1} and 80 mAh g^{-1}) at rapid charge/discharge compared to electrolytes (2) and (3), thereby likely reflecting interphase formation with smaller Ohmic resistances for the underlying

charge transfer as shown in Figure S7a and c (Supporting Information), especially considering that all electrolytes exhibit similar lithium-ion conductivities at 20 °C (σ_{Li+} ~0.04 mS cm^{-1} shown in **Figure 5**c). However, cells operated with both electrolytes encounter unanticipated short circuits, in particular in case of electrolyte (4) where cell failures readily occur within 50 cycles, whereas cells cycling with the other electrolytes remain rather stable over hundred cycles. Note that upon increased operational temperature, the lithium ion transport is boosted (displayed in Figure 5c); nevertheless, the increment of Li^+ conductivity of the electrolyte (2) is relatively less pronounced, attributed to higher cross-linking density and the presence of ether oxygens exhibiting a higher donor number, thereby affording somewhat stronger coordination to lithium ions that eventually hinders the lithium ion diffusion, in this way yielding smaller t_+ values (e.g. t_+ of 0.51, 0.32, 0.34, and 0.40 ±0.02 at 60 °C in the cases of electrolytes (1)-(4), respectively).[54] In theory, the electrochemical cell performance may be improved when exploiting the considered electrolytes at elevated temperatures owing to enhanced ionic conductivities and decreased resistances at the interfaces (see Figure S7b and c; Supporting Information);[55] however, a sudden termination of cycling still occurs (at the 205th cycle; **Figure 5**b) in the case of electrolyte (4) during long-term rapid cycling at 60 °C. Prior to short circuits emerging at both temperature conditions, strong capacity fading is not really observed, thus implying absence of noteworthy electrolyte decompositions upon cycling.[56, 57] Also, a suitable oxidative stability window ~4.4 V is identified (in Figure S8, Supporting Information), highlighting that the stability of the electrolytes against the NMC622 cathode active material is not the major cause that leads to this consequence. Overall, it is possible to attribute the cell failures to consequences of either limited mechanical resistance against electrolyte membrane deformation or localized inhomogeneity of electrolyte constituents within the polymer (as aforementioned) and thus uneven distribution of electrochemical properties that eventually contributes to heterogeneous lithium deposition upon cycling.[58-60]

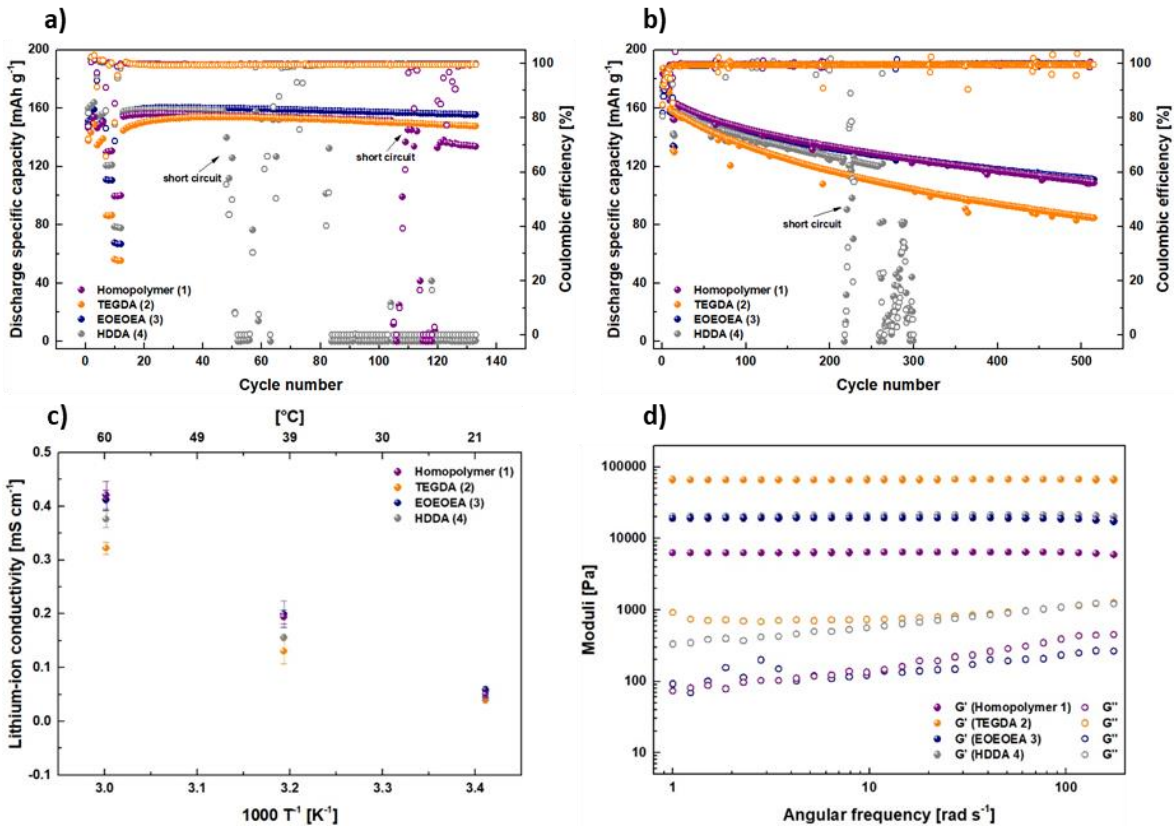

Figure 5. Cycling performance of NMC622||Li cells at a) 20 °C and b) 60 °C with electrolytes (1)-(4), respectively. Formation steps including 0.1/0.2/0.5/1C (3 cycles for each rate) were applied, and the long-term cycling was proceeded at 0.2C for 120 cycles at 20 °C; formation steps of 0.1/0.2/0.5/1/2C and long-term cycling at 1C (~0.4 mA cm^{-2}) were executed at 60 °C. c) Lithium-ion conductivity. d) Storage G' and loss moduli G'' at 20 °C.

On account of compressive mechanical properties which could facilitate HSAL suppression,[59] shear moduli representing the degrees of mechanical resistance to deformation of the polymers, corresponding rheology measurements were performed. As displayed in **Figure 5**d, electrolyte (2) reveals superior mechanical strength (67 kPa) compared to electrolyte (4) (21 kPa) despite possessing similar degrees of cross-linking (as actively controlled by the present number of acryloyl groups). Since the bond energy of C-O (≈92 kcal mol^{-1}) is higher than that of C-C bonds (≈82 kcal mol^{-1}),[61] the actual energy to damage the corresponding polymer membrane is likely also higher, thereby implying that electrolyte (2) offer more reinforced structures against deformation. Electrolyte (4) presents weaker mechanical stability (lesser modulus) and substantially recognizable incompatibility of chemical structures between primary and secondary

segment species (polar and nonpolar), rendering an unambiguous assignment of the origin of cell failures difficult.[59] Note that the observable reinforcement or weakening of the polymer materials mechanical strength is correlated with the cross-linking density.[62-64] Electrolyte (3) is primarily employed for comparison to elucidate likely origins of cell failure when operating electrolyte (4), attributed to the presence of monofunctional EOEOEA instead of bifunctional TEGDA, in this way purposely reducing the degree of cross-linking and mechanical strength (19 kPa) of the resulting membrane.[65, 66] Consequently, comparing to electrolytes (1) and (3), sudden cell failure due to deficient mechanical properties can be excluded for electrolyte (4), since it actually has better mechanical stability. The unanticipated failure of cells operated with electrolyte (1) at 20 °C after a hundred cycles (Figure 5a) may be attributed to insufficient mechanical properties rather than membrane inhomogeneity of homopolymers.[67] The obtained cycling results are in good agreement with the data of corresponding AFM images and MD simulations (Figure 3 and Figure 4) and support the notion that incompatibility between polymer segment species determines the actual distribution of membrane properties that eventually yield locally disparate lithium-ion transport rates that in turn might promote agglomerated lithium deposits and protrusions upon electrochemical cycling.

Morphologies of deposited lithium and stability of SEI

To evaluate the morphology of ill-defined localized lithium deposits reflecting any inhomogeneity of the electrolyte membranes, SEM is a straightforward tool. The images display that lithium surfaces of cells operated with the electrolytes (1) and (3) exhibit comparable morphologies of 2D-planar lithium deposits after long-term cycling in full cells at 60 °C (**Figure 6**a,b), while the lithium surface of cells cycled with electrolyte (4) rather have more localized nuclei

of lithium deposits, even exhibiting dendritic shapes (**Figure 6**c), essentially corroborating that cell failure in case of electrolyte (4) is solely due to inhomogeneous lithium deposition.

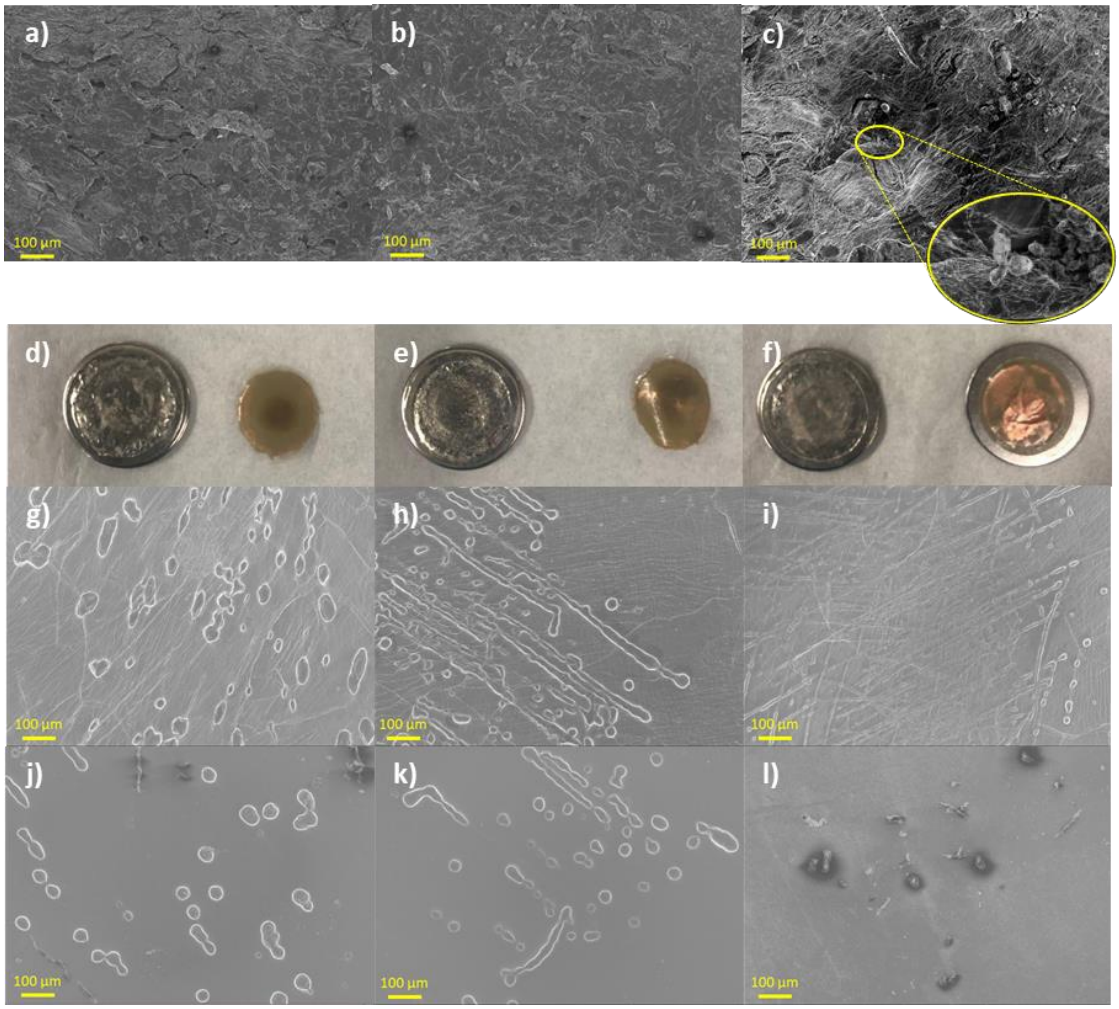

Figure 6. a-c) SEM images of lithium surfaces after long-term cycling performance (500 cycles at 1C) of NMC622||Li cells at 60 °C with the electrolytes of (1), (3) and (4). Images of d-f) dissembled Cu||Li cells and g-l) SEM images after single-side plating with the electrolytes of (1), (3) and (4), respectively. Top view of g-i) stripped lithium surfaces and j-l) polymer membranes covering on plated Cu substrate.

In view of careful validation that instability of SEI layers is also not likely the major factor causing cell failure in case of electrolyte (4), Cu||Li cells with corresponding electrolytes are employed to monitor irreversible electrochemical reactions during cycling.[68] As illustrated in **Figure 7**a-c, cells with electrolyte (4) rapidly experience unanticipated short circuit within 44 cycles, whereas cells with the electrolyte (1) and electrolyte (3) show rather stable performance over two hundred cycles. Since the average values of Coulombic efficiency (CE) prior to cell

failure (before the 44th cycle) are similar among the three considered electrolyte materials ((1): 83%, (3): 83.7%, and (4): 83.3%), it may be concluded that the morphologies and distribution of deposited lithium instead of instability of SEI and "dead lithium" formations determine cell longevity in this system.[47]

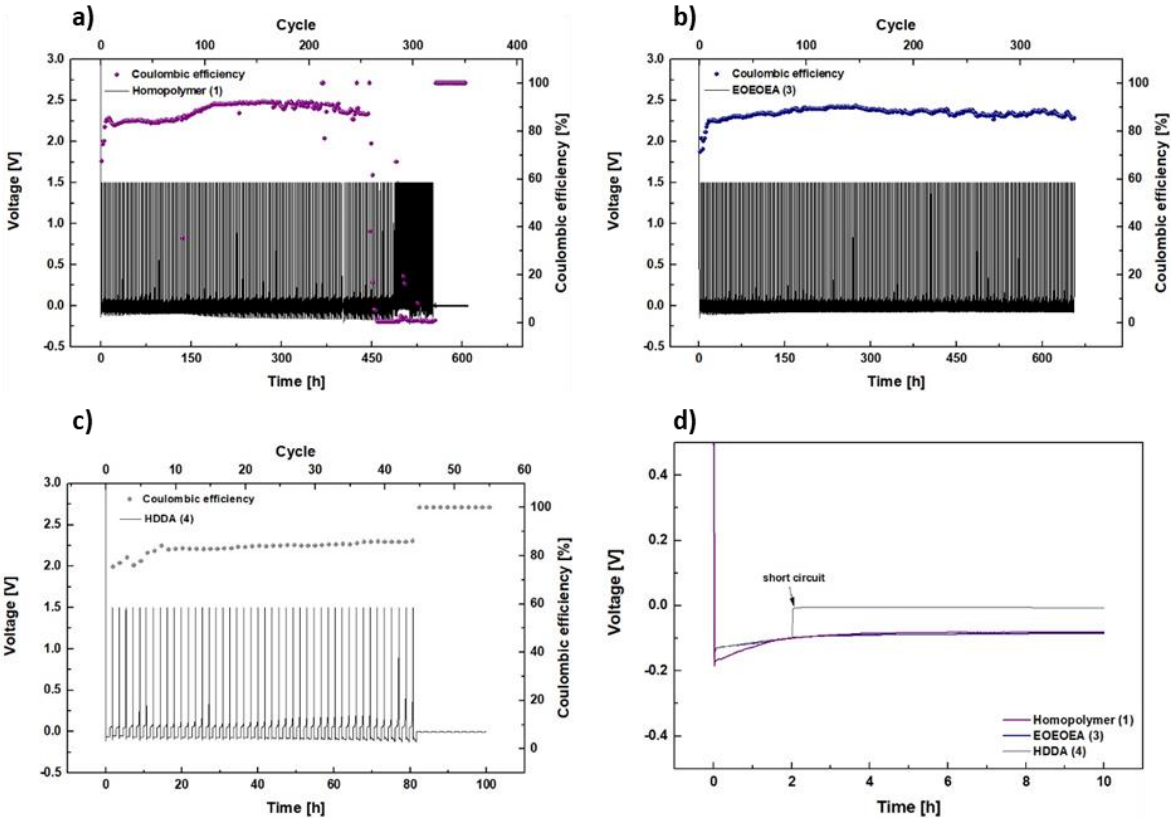

Figure 7. The results of Cu||Li cells with electrolytes of a) (1), b) (3) and c) (4) cycling at 0.1 mA cm^{-2} (1 h per half cycle, cut-off voltage at 1.5 V) and 20 °C. d) The result of single-side plating for 10 h at 0.2 mA cm^{-2} (0.41 mg deposited lithium on Cu) and 20 °C.

Single-side lithium plating onto Cu at higher current density (0.2 mA cm^{-2}) was executed at 20 °C for 10 h to obtain a clearer difference of deposited lithium morphologies between samples. As displayed in **Figure 7**d, cell operation with electrolytes (4) in the worst case was terminated after merely 2 h plating (0.08 mg deposited lithium on Cu) due to a short circuit, while electrolytes (1) and (3) allowed operation for periods of >10 h (0.41 mg deposited lithium on Cu). Additional data of single-side plating of electrolytes (2) and (3) in Li||Li cells is provided in Figure S9 (Supporting Information). Afterwards, Cu||Li cells were carefully dissembled for SEM inspection. In **Figure**

6d-f, it is noticed that the distribution of deposited lithium onto Cu in cells operated with electrolyte (4) appears rather concentrated in certain areas, and most other areas of the electrode surface remain "clean", yet the lithium deposits are evenly spread in case of the other two electrolytes. For electrolyte (4), the corresponding SEM images (**Figure 6**g-i) display that cavities of the lithium-stripped surface are not so pronounced when compared to the other electrolytes due to short circuit. As illustrated in **Figure 6**j-l, distinguishable differences can be readily observed for lithium deposit morphologies under each polymer membrane, especially in case of electrolyte (4) where small fractions of localized and dendritic lithium piercing the membrane are identified (an overview of membrane shown in Figure S10, Supporting Information), suggesting that the cell failures originate from membrane inhomogeneity.

Besides SEM data, ^{7}Li solid state NMR enables monitoring of lithium deposit morphologies based on characteristic chemical shifts of the individual lithium microstructures ("dendritic" (~270 µm), "mossy" (~260 µm) or "smooth" (~245 µm)).[47, 69] After single-side lithium plating onto Cu at a current density of 0.2 mA cm^{-2}, Cu||Li cells were disassembled, and Cu substrates were subjected to ^{7}Li NMR measurements (**Figure 8**a). The result highlights that though the lithium deposits mostly exhibit "smooth" and "mossy" microstructures in case of both polymer electrolytes, the ^{7}Li NMR signals in case of electrolyte (4) appear broader, and the peak extends towards higher chemical shifts. Slightly higher fractions of "mossy" deposits (13.7%) also indicate that the detected lithium metal deposits are comparatively rough at their surface.

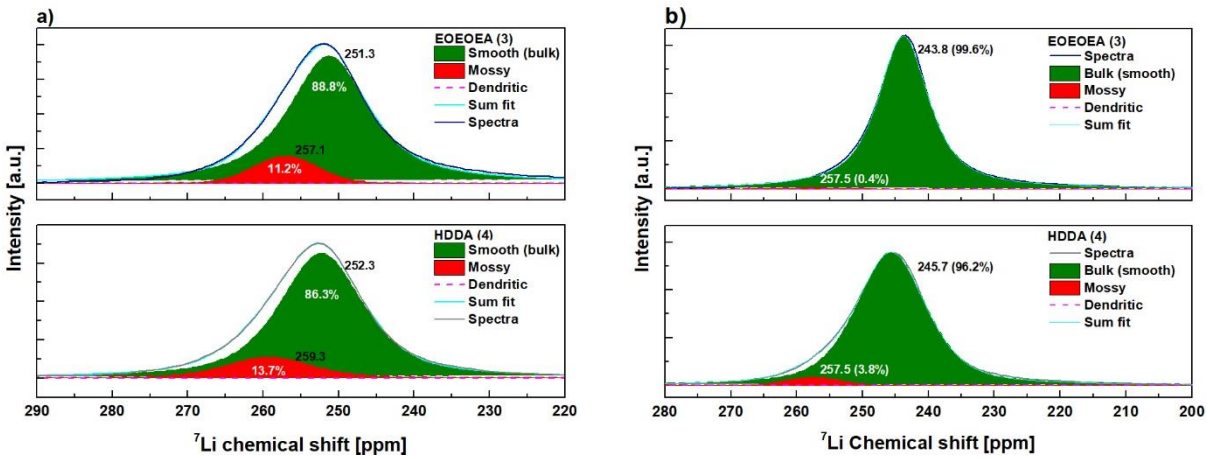

Figure 8. ^{7}Li solid-state NMR spectra (with deconvolution) of a) lithium-plated (~0.16 mg) Cu substrates with electrolytes of (3) and (4) after the operation of single-side plating in Cu||Li coin cells and b) NMC||Li cells measured at the 41th charging state after 40 cycles at 0.2 C and 20 °C.

In another experiment of NMC622||Li cells running for 40 cycles (**Figure 8**b), a similar trend is recognized, showing a wider range of lithium signals and higher fraction of "mossy" deposits (3.8%) in electrolyte (4). Nevertheless, the differences of the corresponding ^{7}Li NMR shifts of the metallic lithium species are not particularly pronounced between the analyzed polymer materials despite that cell instabilities are readily noticeable in case of electrolyte (4) (e.g., voltage noise displayed in Figure S11, Supporting Information), which might be caused by lesser amounts of lithium derived from the thin cathode participating electrochemical cycling. Overall, it is demonstrated that the compatibility between polymer segments not only influences the electrolyte property distributions associated with the consistency of ion transport rate but also determines the homogeneity of lithium deposition and thus the cycling stability.

Improved cell performance due to the decrement of nonpolar bonds of polymer segments

Considering the enhancement of similarity of electrostatic fields between copolymer segments that enables to afford homogeneity of the relevant membrane properties, a slight modification of the series of non-polar carbon bonds of the monomer HDDA may assist to boost the observable cycling performance. This verification was carried out based on a bifunctional monomer of BDDA

as secondary segment species possessing similar C-C covalent bonds as HDDA but with shorter and asymmetric structure that offers more differences between the electrostatic potentials of neighboring atoms while decreasing the number of nonpolar bonds and thereby increasing overall molecular polarity (see **Figure 9**a).[70] The achieved mechanical strength and lithium-ion conductivity of electrolyte (5) are close to the characteristics of electrolyte (4) (see the comparisons in Figure S12, Supporting Information) due to analogous cross-linking densities and similar types of covalent bonds. In view of improved compatibility between the employed polymer segment species, degree of phase separation should be mitigated within electrolyte (5), as shown in **Figure 9**b illustrating the absence of clear phase boundaries (topography image in Figure S4c).

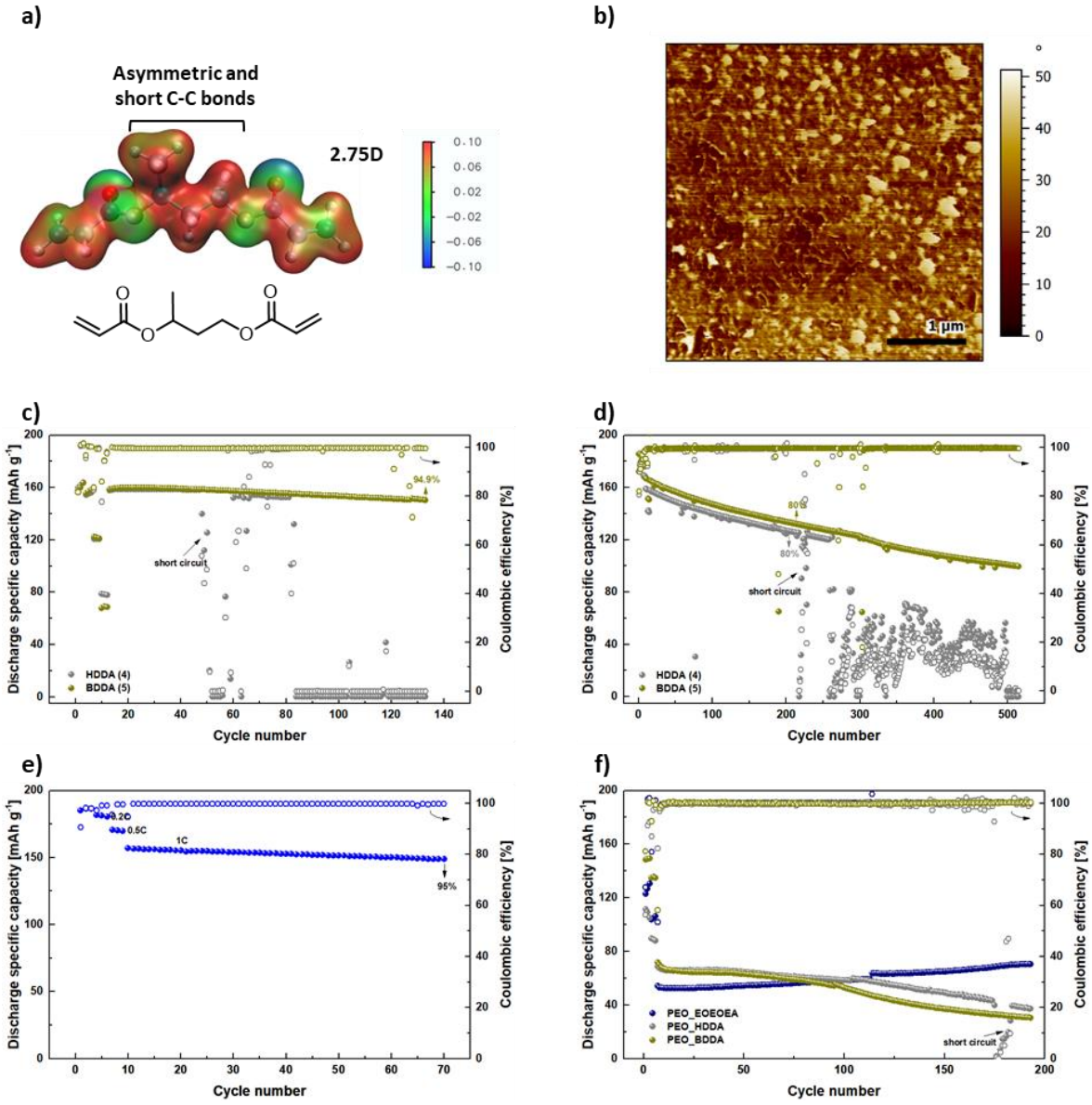

Figure 9. a) Calculated electrostatic potential around each atom on the segment of secondary species BDDA (dipole moment: 2.75D in Boltzmann average); color blue indicates negative potential corresponding to attraction of the proton while color red refers to positive potential corresponding to repulsion of the proton. b) AFM phase image of electrolyte (5). Cycling performance of NMC622||Li cells were conducted at c) 20 °C and d) 60 °C with the electrolyte (5) in comparison with electrolyte (4). At 20 °C: a formation step including 0.1/0.2/0.5/1C (3 cycles for each rate) was applied, and the long-term cycling was proceeded at 0.2C for 120 cycles; at 60 °C: a formation step of 0.1/0.2/0.5/1/2C (3 cycles for each rate) and 1C for long-term performance. e) Cycling performance in thick NMC622 (filtrated with electrolyte (3)) ||Li cell with the optimized electrolyte (3) at 1C and 60 °C. f) Cycling performance in NMC622||Li with PEO-based electrolytes at 0.2 C and 20 °C; formation step: 0.05/0.1C (3 cycles at each rate).

The corresponding cell cycling stability is indeed ameliorated when operating electrolyte (5), clearly emphasizing the impact of better membrane homogeneity, while exhibiting absence of cell short circuits over hundred cycles at both operational temperatures of 20 °C and 60 °C and similar trends of capacity retention compared to electrolyte (4) (**Figure 9**c and d). Moreover, with the

optimized electrolyte (3) in this PTMC-based system, full cycling performance against a thicker cathode (mass loading: 6.3 mg cm^{-2}) is also feasible at 1C and 60 °C, showing quite promising capacity retention (**Figure 9**e). To confirm that the proposed concept is also functioning well in other polymer systems, commonly-used oligomer of poly-(ethylenglykol)-diacrylat (PEGDA) in literatures (Figure 1) was employed to replace PTMC-GCDs as the primary polymer species.[17, 18, 20, 21, 23, 28] In **Figure 9**f, the electrochemical performance of NMC622||Li cells operated with electrolyte PEO_EOEOEA gratually enhaces, likely indicating formation of more effective and robust interphases upon cycling. Likewise, interphase formation in this case may need more more time (>>12 h) for actually achieving equilibrium or metastable conditions. But overall, all cells with the PEO-based electrolytes provide very limited capacity (around 65 mAh g^{-1}), meaning only small amount of lithium can really participate in stripping and plating process; hence, the possibility of forming lithium protrusions that cause cycling termination requires more cycles (e.g., after 175 cycles, the first case of short circuit occurring in PEO_HDDA). Also, data of lithium single-side plating shown in Figure S13 (Supporting Information) reveal instable electrochemical behavior after 62 h in the cells with the PEO-based electrolyte containing HDDA segments and ameliorated performance in the cells with other electrolytes possessing more compatible copolymer segments. In summary, this experimental approach successfully demonstrates that the homogeneity of electrolyte properties affects relevant electrochemical features including cycling performance, e.g., due to non-uniformity of charge carrier transport, thereby introducing an important parameter and strategy towards targeted design of advanced copolymer electrolytes. Note that in future work, a reduction of the cell operation temperatures might be achieved upon combination of segment-tailored polymers with recently introduced thermally responsive electrolytes,[71, 72] creating synergies based on robust and homogeneous SEI formation as well as enhanced thermal stability,

thereby potentially bestowing the ability to delay thermal runaway of the cycled cells, also enabling cell operation at ambient temperatures.

Conclusions

The development of novel polymer electrolytes can involve a tedious series of trial and error attempts that consume time and energy, thus necessitating comprehensive guidelines for tailored electrolyte design. As part of a rational approach to quasi-solid copolymer electrolytes, the impact of structural chemistry of copolymer segments on the reversibility and morphology of lithium metal deposition is elucidated. Indeed, careful selection of reactive monomer and/or oligomer species possessing similar electrostatic fields or polarity in their structures enables to effectively enhance the resulting homogeneity of copolymer electrolyte membranes suitable for operation in lithium metal batteries, in this way controlling the consistency of charge carrier transport and avoiding growth of severely localized lithium protrusions. This notion is not only indicated from the trend of cell longevities in a collection of literatures but also validated in a unique PTMC-based system and generally in PEO-based electrolytes. Overall, the introduced concept facilitates guidance for more systematic tailoring and modeling of structures for future copolymer electrolytes.

Supporting Information

Supporting Information is available, including ^{1}H NMR/GPC data of PTMC-grafted cyclodextrins, schematic representation of network structures, details of DFT and Molecular Dynamics simulation, partial charges of constituents and polymers, structural and RDF data, AFM topography and SEM images, DSC traces and solubility data, Nyquist plots and impedance data from equivalent circuit fitting, conductivities and additional electrochemical data (Li plating, galvanostatic data).

Author Information

Corresponding Authors

Gunther Brunklaus - Forschungszentrum Jülich GmbH, Helmholtz-Institute Münster, IEK-12, Corrensstraße 46, 48149 Münster, Germany; Email: g.brunklaus@fz-juelich.de

Authors

Min-Huei Chiou - Forschungszentrum Jülich GmbH, Helmholtz-Institute Münster, IEK-12, Corrensstraße 46, 48149 Münster, Germany

Elisabeth Verweyen - Forschungszentrum Jülich GmbH, Helmholtz-Institute Münster, IEK-12, Corrensstraße 46, 48149 Münster, Germany

Diddo Diddens - Forschungszentrum Jülich GmbH, Helmholtz-Institute Münster, IEK-12, Corrensstraße 46, 48149 Münster, Germany

Lennart Wichmann - Forschungszentrum Jülich GmbH, Helmholtz-Institute Münster, IEK-12, Corrensstraße 46, 48149 Münster, Germany

Christina Schmidt - Forschungszentrum Jülich GmbH, Helmholtz-Institute Münster, IEK-12, Corrensstraße 46, 48149 Münster, Germany

Kerstin Neuhaus - Forschungszentrum Jülich GmbH, Helmholtz-Institute Münster, IEK-12, Corrensstraße 46, 48149 Münster, Germany

Aditya Choudhary - Department of Materials Science and Engineering, University of Utah, 122 S. Central Campus Dr., Salt Lake City, UT 84112, USA

Dmitry Bedrov - Department of Materials Science and Engineering, University of Utah, 122 S. Central Campus Dr., Salt Lake City, UT 84112, USA

Martin Winter - Forschungszentrum Jülich GmbH, Helmholtz-Institute Münster, IEK-12, Corrensstraße 46, 48149 Münster, Germany; MEET Battery Research Center, University of Münster, Corrensstraße 46, 48149 Münster, Germany

Note

The authors declare no competing financial interest.

Acknowledgement

The authors M.C., M.W., and G.B. gratefully acknowledge generous support by the German Federal Ministry of Education and Research (BMBF) within “FB2-POLY” (13XP0429A) and “LiSI” (13XP0224A). Special thanks to Susanna Krämer for measuring DSC data, Dr. Yi-Chen Hsieh for SEM operation and Dr. Kristina Borzutzki as well as Marvin Mohrhardt for fruitful discussions.

References

1. Yao, P.; Yu, H.; Ding, Z.; Liu, Y.; Lu, J.; Lavorgna, M.; Wu, J.; Liu, X. Review on Polymer-Based Composite Electrolytes for Lithium Batteries. *Frontiers in Chemistry* **2019**, *7*, DOI: 10.3389/fchem.2019.00522
2. Zhang, N.; Du, L.; Zhang, J.; Xu, H.; Zhou, X.; Mai, L.; Xu, L. Self-Assembled Tent-Like Nanocavities for Space-Confined Stable Lithium Metal Anode. *Adv. Funct. Mater.* **2023**, *n/a*, 2210862, DOI: 10.1002/adfm.202210862
3. Li, Q.; Pan, H.; Li, W.; Wang, Y.; Wang, J.; Zheng, J.; Yu, X.; Li, H.; Chen, L. Homogeneous Interface Conductivity for Lithium Dendrite-Free Anode. *ACS Energy Letters* **2018**, *3*, 2259, DOI: 10.1021/acsenergylett.8b01244
4. Xu, H.; Sun, C.; Zhang, S.; Zhang, H.; Liu, Z.; Tang, Y.; Cui, G. A Rigid-Tough Coupling Strategy Engineering Mechanochemically Stable SEI towards Long-Life Lithium Metal Batteries. *ChemSusChem* **2023**, *n/a*, e202202334, DOI: 10.1002/cssc.202202334
5. Chazalviel, J.N. Electrochemical aspects of the generation of ramified metallic electrodeposits. *Phys. Rev. A* **1990**, *42*, 7355, DOI: 10.1103/PhysRevA.42.7355

6. Monroe, C.; Newman, J. The Impact of Elastic Deformation on Deposition Kinetics at Lithium/Polymer Interfaces. *J. Electrochem. Soc.* **2005**, *152*, A396, DOI: 10.1149/1.1850854

7. Khurana, R.; Schaefer, J.L.; Archer, L.A.; Coates, G.W. Suppression of Lithium Dendrite Growth Using Cross-Linked Polyethylene/Poly(ethylene oxide) Electrolytes: A New Approach for Practical Lithium-Metal Polymer Batteries. *J. Am. Chem. Soc.* **2014**, *136*, 7395, DOI: 10.1021/ja502133j

8. Lu, Q.; Fang, J.; Yang, J.; Miao, R.; Wang, J.; Nuli, Y. Novel cross-linked copolymer gel electrolyte supported by hydrophilic polytetrafluoroethylene for rechargeable lithium batteries. *J. Membr. Sci.* **2014**, *449*, 176, DOI: 10.1016/j.memsci.2013.08.029

9. Long, L.; Wang, S.; Xiao, M.; Meng, Y. Polymer electrolytes for lithium polymer batteries. *J. Mater. Chem. A* **2016**, *4*, 10038, DOI: 10.1039/C6TA02621D

10. Young, W.-S.; Kuan, W.-F.; Epps, I., Thomas H. Block copolymer electrolytes for rechargeable lithium batteries. *J. Polym. Sci., Part B: Polym. Phys.* **2014**, *52*, 1, DOI: 10.1002/polb.23404

11. Kambe, Y.; Arges, C.G.; Czaplewski, D.A.; Dolejsi, M.; Krishnan, S.; Stoykovich, M.P.; de Pablo, J.J.; Nealey, P.F. Role of Defects in Ion Transport in Block Copolymer Electrolytes. *Nano Lett.* **2019**, *19*, 4684, DOI: 10.1021/acs.nanolett.9b01758

12. Sharon, D.; Bennington, P.; Dolejsi, M.; Webb, M.A.; Dong, B.X.; de Pablo, J.J.; Nealey, P.F.; Patel, S.N. Intrinsic Ion Transport Properties of Block Copolymer Electrolytes. *ACS Nano* **2020**, *14*, 8902, DOI: 10.1021/acsnano.0c03713

13. Wang, G.; Li, J.; Shang, L.; He, H.; Cui, T.; Chai, S.; Zhao, C.; Wu, L.; Li, H. Nanostructured Polymer Composite Electrolytes with Self-Assembled Polyoxometalate

Networks for Proton Conduction. *CCS Chemistry* **2021**, 1, DOI: 10.31635/ccschem.021.202000608

14. Borzutzki, K.; Dong, K.; Nair, J.R.; Wolff, B.; Hausen, F.; Eichel, R.-A.; Winter, M.; Manke, I.; Brunklaus, G. Lithium deposition in single-ion conducting polymer electrolytes. *Cell Rep. Phys. Sci.* **2021**, *2*, 100496, DOI: 10.1016/j.xcrp.2021.100496
15. Zhang, J.; Farias-Mancilla, B.; Destarac, M.; Schubert, U.S.; Keddie, D.J.; Guerrero-Sanchez, C.; Harrisson, S. Asymmetric Copolymers: Synthesis, Properties, and Applications of Gradient and Other Partially Segregated Copolymers. *Macromol. Rapid Commun.* **2018**, *39*, 1800357, DOI: 10.1002/marc.201800357
16. Ramos-Garcés, M.V.; Li, K.; Lei, Q.; Bhattacharya, D.; Kole, S.; Zhang, Q.; Strzalka, J.; Angelopoulou, P.P.; Sakellariou, G.; Kumar, R.; Arges, C.G. Understanding the ionic activity and conductivity value differences between random copolymer electrolytes and block copolymer electrolytes of the same chemistry. *RSC Adv.* **2021**, *11*, 15078, DOI: 10.1039/D1RA02519H
17. Song, M.-K.; Cho, J.-Y.; Cho, B.W.; Rhee, H.-W. Characterization of UV-cured gel polymer electrolytes for rechargeable lithium batteries. *J. Power Sources* **2002**, *110*, 209, DOI: 10.1016/S0378-7753(02)00258-6
18. Cheng, C.L.; Wan, C.C.; Wang, Y.Y. Preparation of porous, chemically cross-linked, PVdF-based gel polymer electrolytes for rechargeable lithium batteries. *J. Power Sources* **2004**, *134*, 202, DOI: 10.1016/j.jpowsour.2004.03.037
19. Choi, N.-S.; Park, J.-K. A comparative study of coordination between host polymers and Li+ ions in UV-cured gel polymer electrolytes. *Solid State Ion.* **2009**, *180*, 1204, DOI: 10.1016/j.ssi.2009.06.005

20. Shi, J.; Hu, H.; Xia, Y.; Liu, Y.; Liu, Z. Polyimide matrix-enhanced cross-linked gel separator with three-dimensional heat-resistance skeleton for high-safety and high-power lithium ion batteries. *J. Mater. Chem. A* **2014**, *2*, 9134, DOI: 10.1039/C4TA00808A

21. Lu, Q.; Yang, J.; Lu, W.; Wang, J.; Nuli, Y. Advanced semi-interpenetrating polymer network gel electrolyte for rechargeable lithium batteries. *Electrochim. Acta* **2015**, *152*, 489, DOI: 10.1016/j.electacta.2014.11.176

22. Chaudoy, V.; Ghamouss, F.; Luais, E.; Tran-Van, F. Cross-Linked Polymer Electrolytes for Li-Based Batteries: From Solid to Gel Electrolytes. *Ind. Eng. Chem. Res.* **2016**, *55*, 9925, DOI: 10.1021/acs.iecr.6b02287

23. Fan, W.; Li, N.-W.; Zhang, X.; Zhao, S.; Cao, R.; Yin, Y.; Xing, Y.; Wang, J.; Guo, Y.-G.; Li, C. A Dual-Salt Gel Polymer Electrolyte with 3D Cross-Linked Polymer Network for Dendrite-Free Lithium Metal Batteries. *Advanced Science* **2018**, *5*, 1800559, DOI: 10.1002/advs.201800559

24. Baik, J.-H.; Kim, S.; Hong, D.G.; Lee, J.-C. Gel Polymer Electrolytes Based on Polymerizable Lithium Salt and Poly(ethylene glycol) for Lithium Battery Applications. *ACS Appl. Mater. Interfaces* **2019**, *11*, 29718, DOI: 10.1021/acsami.9b05139

25. Dai, K.; Ma, C.; Feng, Y.; Zhou, L.; Kuang, G.; Zhang, Y.; Lai, Y.; Cui, X.; Wei, W. A borate-rich, cross-linked gel polymer electrolyte with near-single ion conduction for lithium metal batteries. *J. Mater. Chem. A* **2019**, *7*, 18547, DOI: 10.1039/C9TA05938E

26. Xiao, Q.; Deng, C.; Wang, Q.; Zhang, Q.; Yue, Y.; Ren, S. In Situ Cross-Linked Gel Polymer Electrolyte Membranes with Excellent Thermal Stability for Lithium Ion Batteries. *ACS Omega* **2019**, *4*, 95, DOI: 10.1021/acsomega.8b02255

27. Ahmed, F.; Kim, D.; Lei, J.; Ryu, T.; Yoon, S.; Zhang, W.; Lim, H.; Jang, G.; Jang, H.; Kim, W. UV-Cured Cross-Linked Astounding Conductive Polymer Electrolyte for Safe

and High-Performance Li-Ion Batteries. *ACS Appl. Mater. Interfaces* **2021**, *13*, 34102, DOI: 10.1021/acsami.1c06233

28. Long, M.-C.; Wang, T.; Duan, P.-H.; Gao, Y.; Wang, X.-L.; Wu, G.; Wang, Y.-Z. Thermotolerant and fireproof gel polymer electrolyte toward high-performance and safe lithium-ion battery. *Journal of Energy Chemistry* **2022**, *65*, 9, DOI: 10.1016/j.jechem.2021.05.027

29. Wang, Q.; Zhang, P.; Zhu, W.; Zhang, D.; Li, Z.; Wang, H.; Sun, H.; Wang, B.; Fan, L.-Z. A two-step strategy for constructing stable gel polymer electrolyte interfaces for long-life cycle lithium metal batteries. *Journal of Materiomics* **2022**, *8*, 1048, DOI: 10.1016/j.jmat.2022.02.009

30. Chiou, M.-H.; Borzutzki, K.; Thienenkamp, J.H.; Mohrhardt, M.; Liu, K.-L.; Mereacre, V.; Binder, J.R.; Ehrenberg, H.; Winter, M.; Brunklaus, G. Durable fast-charging lithium metal batteries designed with cross-linked polymer electrolytes and niobate-coated cathode. *J. Power Sources* **2022**, *538*, 231528, DOI: 10.1016/j.jpowsour.2022.231528

31. Frisch, M.J.; Trucks, G.W.; Schlegel, H.B.; Scuseria, G.E.; Robb, M.A.; Cheeseman, J.R.; Scalmani, G.; Barone, V.; Petersson, G.A.; Nakatsuji, H.; Li, X.; Caricato, M.; Marenich, A.V.; Bloino, J.; Janesko, B.G.; Gomperts, R.; Mennucci, B.; Hratchian, H.P.; Ortiz, J.V.; Izmaylov, A.F.; Sonnenberg, J.L.; Williams; Ding, F.; Lipparini, F.; Egidi, F.; Goings, J.; Peng, B.; Petrone, A.; Henderson, T.; Ranasinghe, D.; Zakrzewski, V.G.; Gao, J.; Rega, N.; Zheng, G.; Liang, W.; Hada, M.; Ehara, M.; Toyota, K.; Fukuda, R.; Hasegawa, J.; Ishida, M.; Nakajima, T.; Honda, Y.; Kitao, O.; Nakai, H.; Vreven, T.; Throssell, K.; Montgomery Jr., J.A.; Peralta, J.E.; Ogliaro, F.; Bearpark, M.J.; Heyd, J.J.; Brothers, E.N.; Kudin, K.N.; Staroverov, V.N.; Keith, T.A.; Kobayashi, R.; Normand, J.; Raghavachari, K.; Rendell, A.P.; Burant, J.C.; Iyengar, S.S.; Tomasi, J.; Cossi, M.; Millam, J.M.; Klene, M.; Adamo,

C.; Cammi, R.; Ochterski, J.W.; Martin, R.L.; Morokuma, K.; Farkas, O.; Foresman, J.B.; Fox, D.J., *Gaussian 16 Rev. C.01*. 2016: Wallingford, CT.

32. Marenich, A.V.; Cramer, C.J.; Truhlar, D.G. Universal Solvation Model Based on Solute Electron Density and on a Continuum Model of the Solvent Defined by the Bulk Dielectric Constant and Atomic Surface Tensions. *J. Phys. Chem. B* **2009**, *113*, 6378, DOI: 10.1021/jp810292n

33. Borodin, O.; Behl, W.; Jow, T.R. Oxidative Stability and Initial Decomposition Reactions of Carbonate, Sulfone, and Alkyl Phosphate-Based Electrolytes. *The Journal of Physical Chemistry C* **2013**, *117*, 8661, DOI: 10.1021/jp400527c

34. Borodin, O.; Olguin, M.; Spear, C.E.; Leiter, K.W.; Knap, J. Towards high throughput screening of electrochemical stability of battery electrolytes. *Nanotechnology* **2015**, *26*, 354003, DOI: 10.1088/0957-4484/26/35/354003

35. Hall, D.S.; Self, J.; Dahn, J.R. Dielectric Constants for Quantum Chemistry and Li-Ion Batteries: Solvent Blends of Ethylene Carbonate and Ethyl Methyl Carbonate. *The Journal of Physical Chemistry C* **2015**, *119*, 22322, DOI: 10.1021/acs.jpcc.5b06022

36. Melitz, W.; Shen, J.; Kummel, A.C.; Lee, S. Kelvin probe force microscopy and its application. *Surf. Sci. Rep.* **2011**, *66*, 1, DOI: 10.1016/j.surfrep.2010.10.001

37. Borodin, O. Polarizable Force Field Development and Molecular Dynamics Simulations of Ionic Liquids. *J. Phys. Chem. B* **2009**, *113*, 11463, DOI: 10.1021/jp905220k

38. Bedrov, D.; Piquemal, J.-P.; Borodin, O.; MacKerell, A.D., Jr.; Roux, B.; Schröder, C. Molecular Dynamics Simulations of Ionic Liquids and Electrolytes Using Polarizable Force Fields. *Chem. Rev.* **2019**, *119*, 7940, DOI: 10.1021/acs.chemrev.8b00763

39. Choudhary, A.; Dong, D.; Bedrov, D. Li+ Transport in Ethylene Carbonate Based Comb-Branched Solid Polymer Electrolyte: A Molecular Dynamics Simulation Study. *ACS Applied Polymer Materials* **2022**, *4*, 8496, DOI: 10.1021/acsapm.2c01416

40. Dong, D.; Choudhary, A.; Bedrov, D. Coupling–Decoupling Transition between Li+ Transport and Segmental Relaxation in Solid Polymer Electrolytes. *ACS Applied Polymer Materials* **2020**, *2*, 5358, DOI: 10.1021/acsapm.0c01029

41. Chen, Y.-H.; Hsieh, Y.-C.; Liu, K.L.; Wichmann, L.; Thienenkamp, J.H.; Choudhary, A.; Bedrov, D.; Winter, M.; Brunklaus, G. Green Polymer Electrolytes Based on Polycaprolactones for Solid-State High-Voltage Lithium Metal Batteries. *Macromol. Rapid Commun.* **2022**, *43*, 2200335, DOI: 10.1002/marc.202200335

42. Thole, B.T. Molecular polarizabilities calculated with a modified dipole interaction. *Chem. Phys.* **1981**, *59*, 341, DOI: 10.1016/0301-0104(81)85176-2

43. Palmer, B.J. Direct Application of Shake to the Velocity Verlet Algorithm. *J. Comput. Phys.* **1993**, *104*, 470, DOI: 10.1006/jcph.1993.1045

44. Hoover, W.G. Canonical dynamics: Equilibrium phase-space distributions. *Phys. Rev. A* **1985**, *31*, 1695, DOI: 10.1103/PhysRevA.31.1695

45. Evans, D.J.; Holian, B.L. The Nose–Hoover thermostat. *J. Chem. Phys.* **1985**, *83*, 4069, DOI: 10.1063/1.449071

46. Martyna, G.J.; Tuckerman, M.E.; Tobias, D.J.; Klein, M.L. Explicit reversible integrators for extended systems dynamics. *Mol. Phys.* **1996**, *87*, 1117, DOI: 10.1080/00268979600100761

47. Hsieh, Y.-C.; Leißing, M.; Nowak, S.; Hwang, B.-J.; Winter, M.; Brunklaus, G. Quantification of Dead Lithium via In Situ Nuclear Magnetic Resonance Spectroscopy. *Cell Rep. Phys. Sci.* **2020**, *1*, 100139, DOI: 10.1016/j.xcrp.2020.100139

48. Nishimoto, A.; Watanabe, M.; Ikeda, Y.; Kohjiya, S. High ionic conductivity of new polymer electrolytes based on high molecular weight polyether comb polymers. *Electrochim. Acta* **1998**, *43*, 1177, DOI: 10.1016/S0013-4686(97)10017-2

49. Dvir, H.; Jopp, J.; Gottlieb, M. Estimation of polymer–surface interfacial interaction strength by a contact AFM technique. *J. Colloid Interface Sci.* **2006**, *304*, 58, DOI: 10.1016/j.jcis.2006.08.053

50. Li, L.; Chan, C.-M.; Yeung, K.L.; Li, J.-X.; Ng, K.-M.; Lei, Y. Direct Observation of Growth of Lamellae and Spherulites of a Semicrystalline Polymer by AFM. *Macromolecules* **2001**, *34*, 316, DOI: 10.1021/ma000273e

51. Graaf, L.; Möller, M. Glass transition temperatures of microphase-separated semi-interpenetrating polymer networks of polystyrene-inter-poly(cross-2-ethylhexyl methacrylate). *Polymer* **1995**, *36*, 3451, DOI: 10.1016/0032-3861(95)92015-7

52. Tanaka, K.; Takahara, A.; Kajiyama, T. Surface molecular motion in thin films of poly(styrene-block-methyl methacrylate) diblock copolymer. *Acta Polym.* **1995**, *46*, 476, DOI: 10.1002/actp.1995.010460612

53. Jung, R.; Metzger, M.; Maglia, F.; Stinner, C.; Gasteiger, H.A. Oxygen Release and Its Effect on the Cycling Stability of LiNixMnyCozO2(NMC) Cathode Materials for Li-Ion Batteries. *J. Electrochem. Soc.* **2017**, *164*, A1361, DOI: 10.1149/2.0021707jes

54. Kim, C.S.; Oh, S.M. Importance of donor number in determining solvating ability of polymers and transport properties in gel-type polymer electrolytes. *Electrochim. Acta* **2000**, *45*, 2101, DOI: 10.1016/S0013-4686(99)00426-0

55. Liu, K.; Liu, M.; Cheng, J.; Dong, S.; Wang, C.; Wang, Q.; Zhou, X.; Sun, H.; Chen, X.; Cui, G. Novel cellulose/polyurethane composite gel polymer electrolyte for high

performance lithium batteries. *Electrochim. Acta* **2016**, *215*, 261, DOI: 10.1016/j.electacta.2016.08.076

56. Lee, H.; Lim, H.-S.; Ren, X.; Yu, L.; Engelhard, M.H.; Han, K.S.; Lee, J.; Kim, H.-T.; Xiao, J.; Liu, J.; Xu, W.; Zhang, J.-G. Detrimental Effects of Chemical Crossover from the Lithium Anode to Cathode in Rechargeable Lithium Metal Batteries. *ACS Energy Letters* **2018**, *3*, 2921, DOI: 10.1021/acsenergylett.8b01819

57. Lee, H.; Lee, D.J.; Kim, Y.-J.; Park, J.-K.; Kim, H.-T. A simple composite protective layer coating that enhances the cycling stability of lithium metal batteries. *J. Power Sources* **2015**, *284*, 103, DOI: 10.1016/j.jpowsour.2015.03.004

58. Yang, M.; Jue, N.; Chen, Y.; Wang, Y. Improving Cyclability of Lithium Metal Anode via Constructing Atomic Interlamellar Ion Channel for Lithium Sulfur Battery. *Nanoscale Research Letters* **2021**, *16*, 52, DOI: 10.1186/s11671-021-03508-z

59. Barai, P.; Higa, K.; Srinivasan, V. Lithium dendrite growth mechanisms in polymer electrolytes and prevention strategies. *Phys. Chem. Chem. Phys.* **2017**, *19*, 20493, DOI: 10.1039/C7CP03304D

60. Harry, K.J.; Higa, K.; Srinivasan, V.; Balsara, N.P. Influence of Electrolyte Modulus on the Local Current Density at a Dendrite Tip on a Lithium Metal Electrode. *J. Electrochem. Soc.* **2016**, *163*, A2216, DOI: 10.1149/2.0191610jes

61. Politzer, P.; Ranganathan, S. Bond-order-bond-energy correlations. *Chem. Phys. Lett.* **1986**, *124*, 527, DOI: 10.1016/0009-2614(86)85069-2

62. Nielsen, L.E. Cross-Linking–Effect on Physical Properties of Polymers. *Journal of Macromolecular Science, Part C* **1969**, *3*, 69, DOI: 10.1080/15583726908545897

63. Shokuhfar, A.; Arab, B. The effect of cross linking density on the mechanical properties and structure of the epoxy polymers: molecular dynamics simulation. *J. Mol. Model.* **2013**, *19*, 3719, DOI: 10.1007/s00894-013-1906-9

64. Jeon, O.; Song, S.J.; Lee, K.-J.; Park, M.H.; Lee, S.-H.; Hahn, S.K.; Kim, S.; Kim, B.-S. Mechanical properties and degradation behaviors of hyaluronic acid hydrogels cross-linked at various cross-linking densities. *Carbohydr. Polym.* **2007**, *70*, 251, DOI: 10.1016/j.carbpol.2007.04.002

65. Zhang, L.; Rowan, S.J. Effect of Sterics and Degree of Cross-Linking on the Mechanical Properties of Dynamic Poly(alkylurea–urethane) Networks. *Macromolecules* **2017**, *50*, 5051, DOI: 10.1021/acs.macromol.7b01016

66. Li, C.; Strachan, A. Free volume evolution in the process of epoxy curing and its effect on mechanical properties. *Polymer* **2016**, *97*, 456, DOI: 10.1016/j.polymer.2016.05.059

67. Duan, H.; Yin, Y.-X.; Shi, Y.; Wang, P.-F.; Zhang, X.-D.; Yang, C.-P.; Shi, J.-L.; Wen, R.; Guo, Y.-G.; Wan, L.-J. Dendrite-Free Li-Metal Battery Enabled by a Thin Asymmetric Solid Electrolyte with Engineered Layers. *J. Am. Chem. Soc.* **2018**, *140*, 82, DOI: 10.1021/jacs.7b10864

68. Xiao, J.; Li, Q.; Bi, Y.; Cai, M.; Dunn, B.; Glossmann, T.; Liu, J.; Osaka, T.; Sugiura, R.; Wu, B.; Yang, J.; Zhang, J.-G.; Whittingham, M.S. Understanding and applying coulombic efficiency in lithium metal batteries. *Nat. Energy* **2020**, *5*, 561, DOI: 10.1038/s41560-020-0648-z

69. Hsieh, Y.-C.; Thienenkamp, J.H.; Huang, C.-J.; Tao, H.-C.; Rodehorst, U.; Hwang, B.J.; Winter, M.; Brunklaus, G. Revealing the Impact of Film-Forming Electrolyte Additives on Lithium Metal Batteries via Solid-State NMR/MRI Analysis. *The Journal of Physical Chemistry C* **2021**, *125*, 252, DOI: 10.1021/acs.jpcc.0c09771

70. Furió, C.; Calatayud, M.L. Difficulties with the Geometry and Polarity of Molecules: Beyond Misconceptions. *J. Chem. Educ.* **1996**, *73*, 36, DOI: 10.1021/ed073p36

71. Jiang, F.-N.; Cheng, X.-B.; Yang, S.-J.; Xie, J.; Yuan, H.; Liu, L.; Huang, J.-Q.; Zhang, Q. Thermoresponsive Electrolytes for Safe Lithium-Metal Batteries. *Adv. Mater.* **2023**, *35*, 2209114, DOI: 10.1002/adma.202209114

72. Zhou, Q.; Dong, S.; Lv, Z.; Xu, G.; Huang, L.; Wang, Q.; Cui, Z.; Cui, G. A Temperature-Responsive Electrolyte Endowing Superior Safety Characteristic of Lithium Metal Batteries. *Adv. Energy Mater.* **2020**, *10*, 1903441, DOI: 10.1002/aenm.201903441